Relaxation processes in a multilevel spin system investigated by linewidth analysis of the multifrequency high-frequency EPR spectra

M. Martinelli,[1] C. A. Massa,[1] L. A. Pardi,[1] V. Bercu,[2] and F. F. Popescu[2]
[1]*Istituto per i Processi Chimico-Fisici, CNR, via G. Moruzzi 1, 56124 Pisa, Italy*
[2]*Department of Physics, University of Bucharest, Magurele, RO-76900, Bucharest, Romania*
(Received 19 October 2001; revised manuscript received 16 May 2002; published 31 January 2003)

The line shape measurements of the high-field high-frequency electron paramagnetic resonance transitions for paramagnetic Pb^{3+} in calcite performed at four frequencies between 95 and 285 GHz as function of temperature are reported. The linewidth analysis is based on a recent theory of relaxation for multilevel spin systems at high temperatures and is used to identify the spin lattice relaxation (SLR) mechanisms at such high microwave frequencies. In comparison with previous results obtained at lower microwave frequencies, this analysis emphasizes for a multilevel spin system two relevant new features: (a) the direct SLR process by modulation of the hyperfine interaction significantly contributes to the linewidths even at room temperature and (b) the SLR time of some simple transitions measured from the linewidth under conditions of negligible saturation could be very different from that measured by the continuous saturation method. The difference between the perpendicular-detected transitions and the parallel-detected transition concerning the contributions of the different SLR processes to the SLR times measured by the two methods mentioned above comes out to be very significant.

DOI: 10.1103/PhysRevB.67.014425 PACS number(s): 76.30.Da, 76.20.+q, 32.70.Jz

I. INTRODUCTION

The applications of the high-frequency high-field electron paramagnetic resonance (HF^2EPR) spectroscopy have been thoroughly illustrated and discussed in the literature.[1–9] Most of the authors agree on a number of real and/or potential advantages offered by HF^2EPR techniques compared to conventional EPR. The potentialities of HF^2EPR in the study of the relaxation mechanisms in paramagnetic systems instead have not been thoroughly explored up to date. HF^2EPR offers the possibility to undertake the study of relaxation mechanisms with a multifrequency approach in a broad range of frequencies and temperatures. This is particularly desirable for multilevel spin systems which show important differences compared to simple two-level spin systems such as those originated by a single unpaired electron without a hyperfine (HF) interaction. An example will presented here that, as a consequence of its simplicity, can be considered a school case in the investigation of the many different mechanisms that can affect the paramagnetic relaxation in a multilevel spin system. The relaxation properties of the Pb^{3+} ion in irradiated calcite will be investigated by linewidth (LWD) analysis of continuous-wave HF^2EPR spectra in a range of frequencies going from 95 to 285 GHz. Due to the $6s^1$ electron configuration of the Pb^{3+} ion, the HF interaction is dominated by the Fermi contact term and is thus unusually large compared to that observed in transition-metal ions.[10–12] The HF interaction of Pb^{3+} in calcite is about 38 GHz,[13] larger than conventional microwave bands (9–35 GHz). Thus, using frequencies in the 95–285 GHz range we were able to study a larger number of transitions than in conventional electron paramagnetic resonance (EPR). The transitions observable at high frequency and those observable in the conventional *X*, *K*, and *Q* bands of the microwave spectrum are reported in Fig. 1. The large HF interaction is very sensitive to some dynamic effects such as those generated by the lattice vibrations. The Pb^{3+} ions substitutionally replace Ca^{2+} ions in the $CaCO_3$ lattice. Since Pb mass is about 5 times that of Ca, the vibrational properties of Pb^{3+} in calcite are characterized by a large-amplitude resonant mode. The latter is in turn the origin of the strong temperature dependence of the EPR linewidths.[13] At relatively high temperatures, the spin lattice relaxation (SLR) times are of the order of 10^{-8}–10^{-9} s or even shorter. These extremely short values represent the main obstacle to the direct measurement of

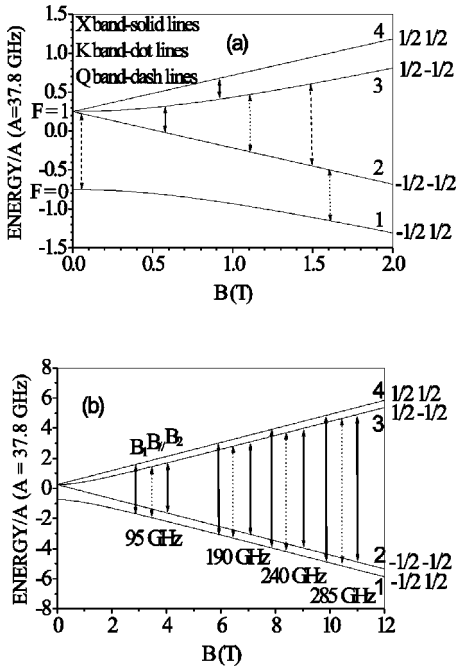

FIG. 1. Energy levels and EPR transitions of Pb^{3+} in calcite. (a) *X*, *K*, and *Q* bands, (b) 95–285 GHz.

the SLR times by standard pulse or cw methods. If the homogeneous broadening mechanisms are dominant, the LWD analysis at high temperatures allows the measurements of the SLR times.[14] The processes operative in electron relaxation are many and often overlapping. For a Kramers doublet, the direct and first-order Raman relaxation mechanisms by modulation of the spin-orbit interaction (MSO) depend strongly on the frequency of the oscillating field. The second-order Raman relaxation processes are, instead, independent of frequency, but strongly dependent on temperature.[12,15] In conventional EPR (9–35 GHz), for diluted paramagnetic solids at relatively high temperatures, only the second-order Raman processes have been put in evidence.[12,14–16] This work will evidence that at high frequency, even at room temperature, the direct relaxation mechanism by modulation of the HF interaction (MHF) significantly contributes to the linewidths.

Three different methods are generally used to measure the SLR time: (i) the saturation recovery method, (ii) the continuous saturation method, and (iii) linewidth analysis under negligible saturation conditions. In the case of an $S=1/2$ spin system with no HF interaction, these three methods give the same result within experimental error. Consequently, in the analysis of SLR for a simple two-level system a unique SLR time T_1 is generally introduced. For a spin system with more than two levels this condition does not hold anymore and the three methods can give different values of the measured SLR times. In the temperature range in which the EPR line corresponding to a simple transition between the levels m and n is homogeneously broadened,[14]

$$(T_2^{mn})^{-1}=(T_2^{SS})^{-1}+({}^{lwd}T_1^{mn})^{-1}, \tag{1.1}$$

where $(T_2^{SS})^{-1}$ and $({}^{lwd}T_1^{mn})^{-1}$ are the contribution to the linewidth of the spin-spin and of the spin-lattice relaxation processes, respectively. The superscript *lwd* indicates the SLR times measured by LWD analysis under negligible saturation. The first is usually temperature independent.[12] For a spin system with a number of levels $K>2$, in the saturation recovery method, the return to equilibrium is described by $K-1$ exponential terms.[15,16] The $K-1$ time constants are not simply related to ${}^{lwd}T_1^{mn}$ or to the ${}^{sat}T_1^{mn}$ measured by the continuous saturation method. ${}^{sat}T_1^{mn}$ and ${}^{lwd}T_1^{mn}$ can in turn be different. For instance, it will be shown that the contribution of the relaxation mechanism by MHF to the SLR times defined above can be very different for some transitions involved in the considered four-level system and, in particular, for the parallel-detected transitions.

II. SPIN SYSTEM AND THE EXPERIMENTAL RESULTS

The calcite single crystals used in the present series of experiments are γ-ray-irradiated specimens (with doses up to 1 Mrad), containing Pb^{3+} as an impurity. The optical and neutron activation analyses[16] have indicated a low concentration of impurities such as Zn, P, and Mn, the most abundant being Pb ($\cong 0.1\%$). The configuration of Pb^{3+} is $6s^1$ and gives rise to an ^2S ground term. The system shows thus nearly isotropic EPR spectra. The ^{207}Pb isotope with $I=\frac{1}{2}$ is present in a percentage of 22.1, while the other isotopes of the metal have $I=0$. The Pb^{3+} EPR spectrum has been studied in the conventional microwave frequency bands in several diamagnetic lattices.[17,18] It has been investigated in calcite in *X*, *K*, and *Q* bands.[13,16]

Calcite contains a combination of elements (Ca, O, C) with a very low natural abundance of nonzero nuclear spin isotopes. As a result, the EPR lines do not show inhomogeneous broadening due to a superhyperfine interaction. In addition, the highly isotropic character of the EPR spectra of Pb^{3+} leads to negligible mosaic structure effects and to isotropic broadening mechanisms. For the LWD analysis this is an important simplification. Consequently, the line shape of the different transitions does not show sizable angular dependence and has a dominant Lorentzian character.

The appropriate spin Hamiltonian for $^{207}Pb^{3+}$ is

$$\hat{H}=\beta\mathbf{B}g\mathbf{S}+\mathbf{B}A\mathbf{I}-g_n\beta_n\mathbf{BI}. \tag{2.1}$$

The first term represents the electronic Zeeman interaction, the second the HF interaction, and the last the nuclear Zeeman interaction. This Hamiltonian can be exactly diagonalized for magnetic field orientations along principal axes[13,19] if the g and A tensors are collinear. When the static magnetic field is along the z axis and $I=S=\frac{1}{2}$ the energy levels of the system are given by the Breit-Rabi formula

$$E_{1,3}=-\frac{A_z}{4}\mp\frac{1}{2}\sqrt{(g_z\beta B)^2(1+\delta)^2+\frac{1}{4}(A_x+A_y)^2}, \tag{2.2a}$$

$$E_{2,4}=\frac{A_z}{4}\mp\frac{1}{2}\sqrt{(g_z\beta B)^2(1-\delta)^2+\frac{1}{4}(A_x-A_y)^2}, \tag{2.2b}$$

where $\delta=g_n\beta_n/g\beta$.

Pb^{3+} in calcite shows an axial EPR spectrum with very small anisotropy. At the *X* band and 77 K the spin Hamiltonian parameters are[13] $g_\parallel=2.0046\pm0.0002$, $A_\parallel=(37.868\pm0.005)$ GHz, $g_\perp-g_\parallel=0.0019\pm0.0002$, and $A_\perp-A_\parallel=(0.030\pm0.001)$ GHz. Therefore, to a good approximation,

$$g_z\cong g_x=g_y=g,\quad A_z\cong A_x=A_y=A. \tag{2.3}$$

In this approximation, the wave functions corresponding to the levels (2.2) are

$$\Psi_{1,3}=\alpha\left|\mp\frac{1}{2},\pm\frac{1}{2}\right\rangle\mp\gamma\left|\pm\frac{1}{2},\mp\frac{1}{2}\right\rangle,\quad \Psi_{2,4}=\left|\mp\frac{1}{2},\mp\frac{1}{2}\right\rangle, \tag{2.4}$$

where the usual $|m_s,m_I\rangle$ set of states was adopted as a basis of the spin space, and where

$$\alpha^2+\gamma^2=1,\quad \alpha^2=\frac{1}{2}\left[1+\frac{g\beta B}{[(g\beta B)^2+A^2]^{1/2}}\right]. \tag{2.5}$$

Let us denote by B_1, B_2, B_3, B_4, and $B_\parallel$ the resonance fields corresponding to the transitions shown in Fig. 1, between the levels 4 and 1, 3 and 2, 2 and 1, 4 and 3, and 3 and 1, respectively, and by B_0, the transition corresponding to

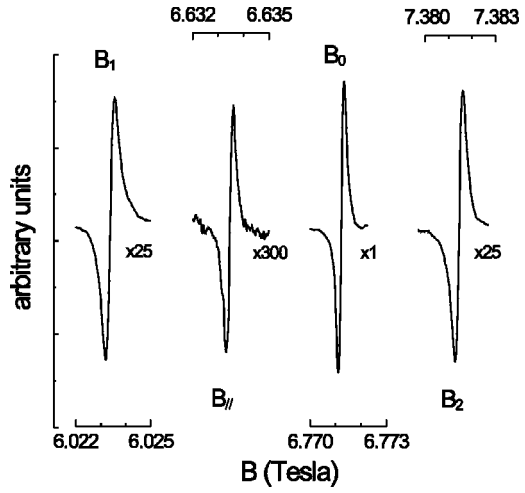

FIG. 2. The EPR spectrum of Pb^{3+} in calcite at 190 GHz and 110 K.

the Kramers doublet due to the Pb isotopes with $I=0$. As shown in Fig. 1(a), because of the large HF splitting, at the *X* band it is possible to observe only the lines at B_0, B_2, and B_4,[13] and in the *K* and *Q* bands those at B_0, B_2, and B_3.[16] At high frequency we observed the lines B_0, B_1, B_2, and $B_\parallel$ [see Figs. 1(b) and 2]. In the following the peak-to-peak linewidths of the above transitions will be denoted as ΔB_i, with $i=0-4$, and $\parallel$.

The EPR measurements have been performed over the range of temperature from 20 K to 300 K and at 95, 190, 240, and 285 GHz using an ultrawide-band EPR spectrometer operative at a HF[2]EPR infrastructure located in Pisa (Italy).[20] The typical appearance of the four main lines of the spectrum at 190 GHz and 100 K is reported in Fig. 2. The spectrometer allows multifrequency experiments by using a single-pass probehead. At 95, 190, and 285 GHz the source is a Gunn effect diode. At 240 GHz we used a homebuilt source: a CO_2-pumped far-infrared (FIR) laser especially optimized for a millimeter band.[20] The magnet system is a superconductor magnet with maximum field of 12 T. The homogeneity of the magnet is about 10 ppm in a 1-cm-diam spherical volume. The sweep coil was used in the low-temperature regime where some of the lines become very narrow.

III. LINE SHAPE ANALYSIS

The line shape of Pb^{3+} EPR spectra in calcite has a dominant Lorentzian character. However, because of the spin Hamiltonian parameter strain caused by local defects in the lattice or by the inhomogeneity of the static magnetic field, the line shape has a degree of inhomogeneous broadening which is reflected in a Gaussian contribution to the linewidth.

In order to analyze the contribution of the SLR processes to the linewidth, one needs to separate the Lorentzian from the Gaussian contribution. Stoneham[21] gave a simple and accurate expression to deconvolute the two contributions. If ΔB_i^L and ΔB_i^G are, respectively, the Lorentzian and Gaussian contributions to the peak-to-peak linewidth of the *i* line ΔB_i, then the expression

$$\Delta B_i=\frac{(\Delta B_i^G)^2+0.8085\Delta B_i^G\Delta B_i^L+0.4621(\Delta B_i^L)^2}{\Delta B_i^G+0.4621\Delta B_i^L} \tag{3.1}$$

gives an accuracy of better than 1% of ΔB_i for both ΔB_i^L and ΔB_i^G.

A. Gaussian contribution

Beyond the contribution given by the strain of the spin Hamiltonian parameters indicated in the following as ΔB_i^{Gc}, other effects can contribute to (ΔB_i^G), which can be consequently expressed as

$$\Delta B_i^G=\sqrt{(\Delta B_i^{Gc})^2+(\Delta B_i^{Gn})^2}. \tag{3.2}$$

ΔB_i^{Gn} can be, for instance, the contribution of the inhomogeneity of the static magnetic field $\Delta B_i^{Gn}=x\cdot B_i$, where *x* depends on the dimension of the sample.

Using approximation (2.3) in Eqs. (2.2), the Gaussian contributions to the linewidths due to the strain of the EPR parameters are[16]

$$\Delta B_0^{Gc}=\left|-\frac{\delta g}{g}B_0\right|, \tag{3.3a}$$

$$\Delta B_{1,2}^{Gc}=\left|-\frac{\delta g}{g}B_{1,2}\mp\frac{\delta A}{2g\beta}\left(1\mp\frac{A}{2h\nu}\right)^{-2}\right|, \tag{3.3b}$$

$$\Delta B_{3,4}^{Gc}=\left|-\frac{\delta g}{g}B_{3,4}\pm\frac{\delta A}{2g\beta}\left(1-\frac{A}{2h\nu}\right)^{-2}\right|, \tag{3.3c}$$

$$\Delta B_\parallel^{Gc}=\left|-\frac{\delta g}{g}B_\parallel-\frac{\delta A}{g\beta}\frac{A}{g\beta B_\parallel}\right|, \tag{3.3d}$$

where δg and δA corresponds to the *g* and *A* strain, respectively. For a given paramagnetic center these strains could be correlated when they have the same physical origin.

B. Lorentzian contribution

The spin-spin relaxation rate $(T_2)^{-1}$ is expressed as a function of the peak-to-peak derivative Lorentzian linewidth ΔB^L by[15,22]

$$(T_2)^{-1}=7.62\times10^6 g\Delta B^L \mathrm{sec}^{-1}, \tag{3.4}$$

where ΔB^L is in gauss, and *g* is the spectroscopic factor. For a multilevel spin manifold, *g* can be defined as $d(h\nu)/\beta dB$, where *B* is the static magnetic field and ν is the frequency of the applied electromagnetic field. Therefore,

$$(T_2)^{-1}=7.62\times10^6 g\Delta B^L\frac{d(h\nu)}{\beta dB}. \tag{3.5}$$

The spin-spin relaxation rates (3.5) of the allowed transitions reported in Fig. 1 become

$$(T_2^{14,23})^{-1}=7.62\times10^6 g\Delta B_{1,2}^L\alpha^2, \tag{3.6a}$$

$$(T_2^{12,34})^{-1}=7.62\times10^6 g\Delta B_{3,4}^L\gamma^2, \tag{3.6b}$$

$$(T_2^{13})^{-1}=7.62\times10^6 g\Delta B_{\|}^L(\alpha^2-\gamma^2). \tag{3.6c}$$

$(T_2^{mn})^{-1}$ represents the Lorentzian linewidth of a simple transition in a frequency sweep experiment, while ΔB_i^L represents the Lorentzian linewidth in a magnetic field sweep experiment.

If the electromagnetic field is near the $m\leftrightarrow n$ resonance, the microwave power absorbed by the sample is

$$P_{mn}=\frac{2(E_m-E_n)(N_m^0-N_n^0)\langle p_{mn}^2\rangle(T_2^{mn})^{-1}}{\Delta\omega_{mn}^2+(T_2^{mn})^{-2}+2\langle p_{mn}^2\rangle(T_2^{mn})^{-1}({}^{sat}T_1^{mn})}, \tag{3.7}$$

where $(T_2^{mn})^{-1}$ is the Lorentzian linewidth given in our case by Eqs. (3.6). ${}^{sat}T_1^{mn}$ is the SLR time measured by the continuous saturation method. E_m, E_n and N_m^0, N_n^0 are, respectively, the energies and populations of the two levels involved in the transition at thermal equilibrium. $\Delta\omega_{mn}$ is the deviation of frequency from the resonance condition and $\langle p_{mn}^2\rangle$ the mean-square value of the Rabi frequency given by

$$\langle p_{14}^2\rangle=\langle p_{23}^2\rangle=\alpha^2\frac{(g\beta b_\perp)^2}{4\hbar^2},$$

$$\langle p_{12}^2\rangle=\langle p_{34}^2\rangle=\gamma^2\frac{(g\beta b_\perp)^2}{4\hbar^2},\quad \langle p_{13}^2\rangle=4\alpha^2\gamma^2\frac{(g\beta b_{||})^2}{4\hbar^2}, \tag{3.8}$$

where $b_\perp$ and $b_\|$ are the perpendicular and parallel components of the applied electromagnetic field with respect to the static magnetic field B.

If the line is not saturated, the Lorentzian linewidth of the $m\leftrightarrow n$ transition can be expressed in terms of the relaxation matrix elements as $(T_2^{mn})^{-1}=-R_{mn}$,[23,24] with

$$R_{mn}=R_{mn}^{SS}+R_{mn}^{SL}, \tag{3.9}$$

where R_{mn}^{SS} and R_{mn}^{SL} represent the spin-spin and spin-lattice contributions, respectively. The second term of the right-hand side in this equation can in turn be expressed as

$$R_{mn}^{SL}=\sum_{p\neq n}R_{np}^{mn}+\sum_{p\neq m}R_{mp}^{mn},$$

where the R_{np}^{mn} are the real parts of the relaxation matrix elements. The pseudodiagonal elements of the relaxation matrix due to the SLR processes are

$$R_{mn}^{mn}=-\frac{1}{2}w_{mn},\quad R_{mn}^{nm}=-\frac{1}{2}w_{nm}, \tag{3.10}$$

with

$$\frac{w_{nm}}{w_{mn}}=\exp\left[\frac{E_n-E_m}{kT}\right], \tag{3.11}$$

where the SLR rate w_{mn} is the sum of two components: (i) w_{mn}^D corresponding to the direct SLR processes and (ii) w_{mn}^R corresponding to the Raman relaxation processes:

$$w_{mn}=w_{mn}^D+w_{mn}^R. \tag{3.12}$$

The off-diagonal elements of the relaxation matrix are

$$R_{np}^{mn}=-\frac{1}{2}w_{np}^D-\frac{1}{2}(1-\chi)w_{np}^R. \tag{3.13}$$

It was demonstrated[25] that the Redfield theory and the theory of relaxation based on the dressed-state formalism are equivalent in the second order of perturbation where, in Eq. (3.13), $\chi=0$. However, it was shown that in the dressed-state formalism, perturbation orders higher than the second give nonvanishing contributions to the off-diagonal elements of the relaxation matrix corresponding to the second-order Raman relaxation mechanism. In this case, in Eq. (3.13), $\chi\cong\frac{1}{2}$. Therefore considering negligible all perturbation terms higher than the second-order terms as assumed by Bloch,[22] Redfield,[23] and Abragam[24] is correct only for a Kramers doublet without a HF interaction. In fact the relaxation matrix for a two-level spin system contains only pseudodiagonal elements, and the condition $\chi=0$ is always verified.

For Pb^{3+}, only two SLR mechanisms are expected to be operative: the first one is originated by MSO and the second by MHF.[16,26] At high temperature,

$$\frac{E_n-E_m}{kT}\ll1, \tag{3.14}$$

and according to Eq. (3.11), $w_{mn}\cong w_{nm}$. For the lead isotopes with $I=0$, the SLR rate is

$$w_{mso}=k_D^2+k_R^2=k^2. \tag{3.15}$$

The first term corresponds to the direct relaxation process by MSO, which involves phonons at the same frequency of the applied electromagnetic field ν. If the condition (3.14) is fulfilled,[12,15]

$$k_D^2=C_D\rho(\nu)\nu^2T, \tag{3.16}$$

where $\rho(\nu)$ is the phonon spectral density of the lattice at the frequency ν. The ν^2 dependence is due to the breaking of the time-reversal symmetry of the Kramers doublet by the electronic Zeeman interaction. The second contribution in Eq. (3.15) is due to the two-phonon relaxation processes. The first- and second-order Raman processes by MSO represented by k_{RI}^2 and k_{RII}^2 have also different sizes. In particular the first is as k_D^2 at a reduced rate of the order $(h\nu/\Delta)^2$, making it usually negligible,[12] Δ being a crystal field splitting. The Raman SLR processes have a strong temperature dependence $f(T)$ and involve the entire phonon spectrum of the lattice[16]:

$$k_R^2\simeq k_{RII}^2=C_Rf(T), \tag{3.17}$$

where k_{RI}^2 has been neglected. From the best fit of the temperature dependence of the EPR linewidths of Pb^{3+} in calcite, $f(T)$ was found to be[16]

$$f(T)\cong\left[\exp\left(\frac{\theta}{T}\right)-1\right]^{-1}, \tag{3.18}$$

which well agrees with the temperature dependence of the HF interaction.[13] This behavior is due to anharmonic effects. These effects are typical for paramagnetic impurities affecting the vibrational properties of the lattice[16,27,28] and, in particular, point to the presence of a large-amplitude resonant mode involving the Pb^{3+} ions.

For Kramers doublets with a large HF interaction, if the condition (3.14) is fulfilled, the corresponding SLR rates are[16]

$$w_{14}\cong w_{41}=\alpha^2k^2,\quad w_{23}\cong w_{32}=\alpha^2k^2, \tag{3.19a}$$

$$w_{12}\cong w_{21}=\gamma^2k^2,\quad w_{34}\cong w_{43}=\gamma^2k^2, \tag{3.19b}$$

$$w_{13}\cong w_{31}\cong w_{mhf}=\alpha^2\gamma^2(\alpha^2-\gamma^2)^2d^2, \tag{3.19c}$$

$$w_{42}\cong w_{24}\cong 0. \tag{3.19d}$$

w_{mhf} is due to the direct and Raman relaxation by MHF (Ref. 26):

$$w_{mhf}=\alpha^2\gamma^2(\alpha^2-\gamma^2)^2d^2,\quad d^2=d_D^2+d_R^2. \tag{3.20}$$

w_{mhf} depends on the steady magnetic field through[26]

$$\alpha^2\gamma^2(\alpha^2-\gamma^2)^2=\frac{(g\beta B)^2A^2}{4[(g\beta B)^2+A^2]^2}. \tag{3.21}$$

It must be pointed out that w_{mhf} is nonvanishing because the wave functions Ψ_1 and Ψ_3 given by Eq. (2.4) corresponding to distinct vibrational levels of the electronic ground state cease to be orthogonal.[26] In this case the SLR rate between these vibrational levels is nonvanishing because the vibrations mix excited states, and the HF interaction corresponding to distinct vibrational levels is not exactly the same. As far as the direct and Raman SLR contributions are concerned one has[12,15]

$$d_D^2=B_D\rho(\nu)T, \tag{3.22a}$$

$$d_R^2=B_Rf(T), \tag{3.22b}$$

where $f(T)$ is given by Eq. (3.18).

The relaxation rates $(T_2^{mn})^{-1}$ are given by Eq. (1.1). Making use of Eqs. (3.10)–(3.22), the SLR times ${}^{lwd}T_1^{mn}$ of the allowed transitions of Pb^{3+} in calcite are given by

$${}^{lwd}(T_1^0)^{-1}={}^{lwd}(T_1^0)_R^{-1}=k^2, \tag{3.23a}$$

$${}^{lwd}(T_1^{14,23})^{-1}={}^{lwd}(T_1^{14})_R^{-1}-\frac{1}{2}\gamma^2k_R^2-\frac{1}{4}\alpha^2\gamma^2(\alpha^2-\gamma^2)^2d_R^2, \tag{3.23b}$$

$${}^{lwd}(T_1^{12,34})^{-1}={}^{lwd}(T_1^{14})_R^{-1}-\frac{1}{2}\alpha^2k_R^2-\frac{1}{4}\alpha^2\gamma^2(\alpha^2-\gamma^2)^2d_R^2, \tag{3.23c}$$

$${}^{lwd}(T_1^{13})^{-1}={}^{lwd}(T_1^{13})_R^{-1}-\frac{1}{2}k_R^2. \tag{3.23d}$$

${}^{lwd}(T_1^{mn})_R^{-1}$ are the values predicted by the Redfield theory:

$${}^{lwd}(T_1^{14,23})_R^{-1}={}^{lwd}(T_1^{12,34})_R^{-1}=k^2+\frac{1}{2}\alpha^2\gamma^2(\alpha^2-\gamma^2)^2d^2, \tag{3.24a}$$

$${}^{lwd}(T_1^{13})_R^{-1}=k^2+\alpha^2\gamma^2(\alpha^2-\gamma^2)^2d^2. \tag{3.24b}$$

The SLR time corresponding to the pair of levels m, n in Eq. (3.7) is ${}^{sat}T_1^{mn}=K_{mn}^n-K_{mn}^m$. The SLR times K_{kj}^i are given by a system of coupled equations[29]

$$\sum_{i\neq m}(-K_{mn}^mw_{mi}+K_{mn}^iw_{im})=\sum_{i\neq n}(K_{mn}^nw_{ni}-K_{mn}^iw_{in})=1,$$

$$\sum_{i\neq j}(K_{mn}^jw_{ji}-K_{mn}^iw_{ij})=0\quad(j\neq m,n). \tag{3.25}$$

By inserting Eq. (3.19) into Eq. (3.25), for $^{207}Pb^{3+}$ isotopes with HF interactions, the SLR times ${}^{sat}T_1^{mn}$ in the approximation (3.14) are[16,26,29]

$${}^{sat}T_1^{12,34}=\frac{1}{k^2}\left[1+\frac{\alpha^2k^2}{2\gamma^2[(\alpha^2-\gamma^2)^2d^2+k^2]}\right], \tag{3.26a}$$

$${}^{sat}T_1^{14,23}=\frac{1}{k^2}\left[1+\frac{\gamma^2k^2}{2\alpha^2[(\alpha^2-\gamma^2)^2d^2+k^2]}\right], \tag{3.26b}$$

$${}^{sat}T_1^{13}=\frac{1}{2\alpha^2\gamma^2[(\alpha^2-\gamma^2)^2d^2+k^2]}, \tag{3.26c}$$

while for Pb^{3+} isotopes without HF interactions,

$${}^{sat}T_1^0=\frac{1}{k^2}. \tag{3.27}$$

IV. ANALYSIS OF THE RELAXATION MECHANISMS

A. *X*, *K*, and *Q* microwave bands

As mentioned in the previous section, the coincidence of ${}^{lwd}T_1^{mn}$ measured under nonsaturation conditions and ${}^{sat}T_1^{mn}$ obtained by continuous saturation method is true only for a Kramers doublet with no HF interaction. Taking into account a recently formulated theory of spin relaxation predicting this fact,[25] the low-frequency EPR spectra of Pb^{3+} in calcite were investigated again using the results of a series of experiments that were previously made in *X*, *K*, and *Q* bands.[16]

TABLE I. Calculated values for the Raman SLR contribution by MHF $\frac{1}{4}d_R^2$ from the LWD analysis at room temperature of the linewidth ΔB_i^{expt} of the EPR transitions in *X*, *K*, and *Q* bands.

Frequency (GHz)	$\Delta B_i^{\text{expt}}(G)$	$\frac{1}{4}d_R^2(G)$
9.43 (*X* band)	$\Delta B_2^{\text{expt}}=20.0\pm0.5$	27.9 ± 5
9.43 (*X* band)	$\Delta B_4^{\text{expt}}=52.0\pm2$	18.6 ± 7.5
24.11 (*K* band)	$\Delta B_2^{\text{expt}}=18.5\pm0.5$	24.7 ± 7
34.43 (*Q* band)	$\Delta B_2^{\text{expt}}=17.0\pm0.5$	23.0 ± 7.5

At relatively high temperature the line shape of B_0 is entirely Lorentzian. Moreover, its linewidth ΔB_0 is independent of frequency and shows a temperature dependence which nicely follows Eq. (3.18); therefore it was concluded that only the second-order Raman relaxation by MSO contributes to the SLR process[12,15] and from Eq. (3.23a) one obtains

$$(T_2^0)^{-1}\cong(T_2^{SS})^{-1}+k_{RII}^2. \tag{4.1}$$

Since $\theta\simeq400$ K, at low temperature, k_{RII}^2 becomes negligible in comparison with $(T_2^{SS})^{-1}$. From the observed linewidth at 77 K, one can find the contribution of the spin-spin relaxation rate as $(T_2^{SS})^{-1}=\Delta B_0^{\text{expt}}(77\text{ K})=(0.60\pm0.05)$G, where 1 G$=1.525\times10^7$ s^{-1}.

The linewidth of the transitions relative to the $^{207}Pb^{3+}$ isotope exhibits a similar temperature dependence as ΔB_0^{expt}. Therefore also in this case, only second-order Raman SLR processes are expected to contribute to the linewidths of the EPR transitions. As for ΔB_0, at low temperature the contributions of the Raman SLR processes to $(T_2^{mn})^{-1}$ are negligible in comparison with $(T_2^{SS})^{-1}$. However, the measured linewidths $\Delta B_2^{\text{expt}}=(1.05\pm0.05)$ G and $\Delta B_4^{\text{expt}}=(4.25\pm0.2)$ G are different from the values predicted by Eqs. (3.6a) and (3.6b) which are 0.8 G, and 3.2 G, respectively. These experimental values were satisfactorily fitted introducing a strain of the HF tensor $\delta A(77\text{ K})=(4.70\pm0.25)$ G in Eqs. (3.3). The validity of this hypothesis was confirmed by high-frequency measurements (see Tables II, III, and IV).

At room temperature $\Delta B_0^{\text{expt}}=(15.0\pm0.5)$ G is constant within error at all the investigated frequencies: namely, 9.43 GHz, 24.11 GHz, and 34.43 GHz. From Eq. (4.1) one obtains $k_R^2(295\text{ K})=(14.4\pm0.5)$ G. The resonance field B_3 in the *Q* band is about 0.2 T. At such value of magnetic field the contribution given by Eq. (3.21) is very small, and the Raman relaxation process by MHF can be neglected. From the measured linewidth $\Delta B_3^{\text{expt}}=(36\pm2)$ G, by using Eq. (3.3c) in Eq. (3.1), the strain of the HF interaction $\delta A(295\text{ K})=(9.0\pm0.5)$ G was found. Taking into account the latter contribution for the observed transition of Fig. 1(a), Eq. (3.23) gives the mean value $d_R^2(295\text{ K})=(94.0\pm10)$ G (see Table I). This value is about 3 times smaller than that obtained if one assumes[16] ${}^{lwd}T_1^{mn}\cong{}^{sat}T_1^{mn}$.

The Redfield theory, corresponding to put $\chi=0$ in Eq. (3.13), is unable to reproduce correctly the experimental data in the Table I. For example, according to Redfield theory, the calculated linewidth ΔB_4 is 80.4 G. Neglecting the contribution of the relaxation by MHF represented by the third term in Eq. (3.23c), one obtains a value of 75 G which is still very different from the observed 52 G. Only by including terms of order higher than the second in the perturbation theory could the observed linewidths reported in Table I be satisfactorily reproduced. One can also obtain a reasonable fit of the observed linewidth replacing in Eq. (1.1) ${}^{lwd}T_1^{mn}$ given by Eqs. (3.23) with ${}^{sat}T_1^{mn}$ given by Eqs. (3.26). In fact, since $({}^{sat}T_1^{mn})^{-1}<({}^{lwd}T_1^{mn})_R^{-1}$, this substitution gives rise to narrower calculated values of the linewidths than those predicted by the Redfield theory. This was actually the hypothesis made in the previous work.[16] It is only the multifrequency spectra and their analysis described in this article that evidenced the contribution of higher-order perturbation terms in the spin relaxation process. As already stated above, such terms correspond to putting $\chi\cong\frac{1}{2}$ in Eq. (3.13).

B. High-frequency high-field analysis

The LWD analysis of the low-frequency spectra reported above gave us some clues about the SLR processes operative in the investigated system and the values of k_R^2, d_R^2, and $(T_2^{SS})^{-1}$. These values will be used hereafter. The transitions observed at high frequency are reported in Fig. 1(b). The LWD analysis of these transitions at different temperatures and frequencies is summarized in Tables II, III, and IV.

1. High-field multifrequency LWD analysis for Pb^{3+} with $I=0$

The temperature dependence of the linewidth of the B_0 transition at high frequency is similar to that found at low frequency. The room-temperature value $\Delta B_0\simeq15$ G is constant within experimental error at all high frequencies. Therefore we can put ${}^{high}T_2^0\cong{}^{low}T_2^0$, where the superscripts *low* and *high* stay for the relaxation times measured at low and high frequencies, respectively. One can thus conclude that the linewidth of the Kramers doublet under conditions of negligible saturation depends, at all frequencies, only on the second-order Raman relaxation originated by MSO. In *X*, *K*, and *Q* bands the broadening mechanism of B_0 is entirely homogeneous and the shape is Lorentzian. Therefore $\Delta B_0^{low}=\Delta B_0^L$. At high frequency, the Lorentzian component ΔB_0^L is the same measured at low frequency. Thus, the Gaussian contribution ΔB_0^G is obtained from Eq. (3.1).

In the low-temperature regime, high-frequency spectra show differences compared to the low-frequency ones. At high magnetic fields, the Gaussian contribution to the linewidth is in fact not negligible and has two components. In order to estimate the relative size of the two components given in Eq. (3.2), two crystals of different volume were used. The two samples will be labeled with the superscripts *I* and *II* in the text and in the tables. Both samples were rhombohedral and of dimensions of about $1\times0.7\times0.3$ cm for *I* and about $1\times1\times0.5$ cm for *II*, having thus roughly 2 times larger volume. For the latter we observed a ΔB_0^{Gn} value 2 times larger than that of the smaller crystal. This proves that ΔB_0^{Gn} is mainly due to the inhomogeneity of the steady magnetic field. These data are reported in Table II, III and IV as ΔB_0^{GnII} and ΔB_0^{GnI} for the larger and smaller crystals, re-

TABLE II. Experimental and calculated linewidths of the EPR spectra of Pb^{3+} in calcite at 95 GHz and 240 GHz and their temperature dependences for sample I.

Frequency (GHz)	95	95	95	95	95	240
T (K)	60^I	110^I	135^I	180^I	295^I	225^I
δA (G)	4.7 ± 0.25	4.8 ± 0.25	5.6 ± 0.25	6.5 ± 0.25		8.0 ± 0.25
ΔB_0^{Gc}(G)	-0.2 ± 0.1	-0.2 ± 0.1	-0.25 ± 0.1	-0.30 ± 0.1	-0.4 ± 0.1	-1.00 ± 0.1
ΔB_0^{GnI}(G)	0.2 ± 0.1	0.2 ± 0.1	0.2 ± 0.1	0.2 ± 0.1	0.2 ± 0.1	0.4 ± 0.2
d_D^2(G)	5.0 ± 6	8 ± 6	12 ± 6	18 ± 6		770 ± 80
ΔB_0^{calc}(G)	0.7	1.25	2.9	6.35	15.0	9.0
ΔB_0^{expt}(G)	0.8 ± 0.1	1.35 ± 0.1	2.9 ± 0.2	6.35 ± 0.2	14.9 ± 1.0	9.0 ± 0.2
ΔB_1^{calc}(G)	3.8	4.30	6.10	9.65		12.45
ΔB_1^{expt}(G)	3.7 ± 0.2	4.15 ± 0.2	5.90 ± 0.2	9.90 ± 0.3		12.6 ± 0.3
ΔB_2^{calc}(G)	2.15	2.60	4.25	7.70		12.15
ΔB_2^{expt}(G)	1.9 ± 0.2	2.75 ± 0.2	4.5 ± 0.2	7.8 ± 0.3		11.9 ± 0.3
$\Delta B_\parallel^{calc}$(G)	2.25	2.60	3.85			
$\Delta B_\parallel^{expt}$(G)	2.4 ± 0.2	2.60 ± 0.2	4.05 ± 0.2			

spectively. ΔB_0^{Gc} is due to the strain of the Zeeman interaction and is given by Eq. (3.3a). This Gaussian contribution increases with a steady magnetic field intensity and temperature. Its values explain why at lower fields the Gaussian contribution ΔB_0^G is negligible.

At $T \leqslant 77$ K, the relaxation rates determined by MSO, k^2, are much lower than $(T_2^{SS})^{-1}$, and they cannot be measured by linewidth analysis. It is well known in fact that at low temperature, the Raman SLR processes become negligible in comparison with the direct processes. The SLR rate corresponding to the direct relaxation process originated by MSO, k_D^2, is reduced by a factor of $(h\nu/\Delta)^2$. Pb^{3+} with a $(6s)^1$ configuration has a ground state which is well isolated from the excited states. Although k_D^2 shows a ν^4 frequency dependence, $h\nu/\Delta$ and consequently k_D^2 are expected to be very small even at the frequencies used in this experiment. At $T < 50$ K the B_0 transition becomes strongly saturated. This fact confirms that the SLR time ${}^{sat}T_1^0$ is very long. In this case the saturation factor in Eq. (3.7) becomes very large, and the line is strongly broadened. In addition, the line shows a Lamb dip especially for the second sample, because in this case the Gaussian contribution is more important.

2. High-field multifrequency LWD analysis of the perpendicular detected transitions for $^{207}Pb^{3+}$

At high frequency the LWD analysis of the EPR spectra relative to the spin multiplet $^{207}Pb^{3+}$ shows new interesting features compared with the low-frequency observation. Besides the contributions of the second-order Raman relaxation mechanisms measured at low frequency, this analysis reveals a direct spin-lattice relaxation process by MHF, d_D^2, given by Eq. (3.22a). For the perpendicular detected transitions,

$$({}^{high}T_2^{14,23})^{-1} \cong ({}^{low}T_2^{23})^{-1} + \frac{1}{2}\alpha^2\gamma^2(\alpha^2-\gamma^2)^2 d_D^2 . \qquad (4.2)$$

TABLE III. Experimental and calculated linewidths of the EPR spectra of Pb^{3+} in calcite at 190 GHz and their temperature dependences for samples I and II.

T (K)	20^I	35^{II}	50^{II}	60^I	110^{II}	140^{II}	175^I	200^{II}	255^{II}	295^I
δA(G)	4.70 ± 0.2	4.70 ± 0.2	4.70 ± 0.2	4.70 ± 0.2	4.8	5.4	6.2 ± 0.25	6.8 ± 0.2	8.1 ± 0.2	9 ± 0.5
ΔB_0^{Gc}(G)	-0.5 ± 0.1	-0.5 ± 0.1	-0.5 ± 0.1	-0.5 ± 0.1	-0.5 ± 0.1	-0.6 ± 0.1	-0.6 ± 0.1	-0.7 ± 0.1	-0.8 ± 0.1	-1.0 ± 0.2
ΔB_0^{GnI}(G)	0.4 ± 0.1			0.4 ± 0.1			0.4 ± 0.1			0.4 ± 0.1
ΔB_0^{GnII}(G)		0.7 ± 0.1	0.7 ± 0.1		0.7 ± 0.1	0.7 ± 0.1		0.7 ± 0.1	0.7 ± 0.1	
d_D^2(G)	35.0 ± 4	60 ± 5	90 ± 10	110 ± 10	200 ± 20	270 ± 25	327 ± 30	360 ± 35	450 ± 45	560 ± 50
ΔB_0^{calc}(G)			1.25	1.0	2.1	3.1	6.35	7.85	11.9	15.0
ΔB_0^{expt}(G)	3.7 ± 0.2		1.25 ± 0.1	1.05 ± 0.1	2.3 ± 0.2	3.2 ± 0.2	6.35 ± 0.2	7.90 ± 0.3	11.9 ± 0.4	15.4 ± 0.5
ΔB_1^{calc}(G)			3.15	3.05	4.15	5.7	8.6	10.6	15.05	18.5
ΔB_1^{expt}(G)	6.2 ± 0.3		3.0 ± 0.2	2.85 ± 0.2	4.2 ± 0.2	5.6 ± 0.3	9.1 ± 0.3	10.1 ± 0.4	15.0 ± 0.5	18.0 ± 0.7
ΔB_2^{calc}(G)			3.0	2.90	3.95	5.0	8.65	10.0	14.35	18.4
ΔB_2^{expt}(G)			2.80 ± 0.2	2.70 ± 0.2	3.8 ± 0.2	5.2 ± 0.3	8.7 ± 0.3	10.0 ± 0.4	14.4 ± 0.5	18.2 ± 0.7
$\Delta B_\parallel^{calc}$(G)	1.35	1.55	1.75	1.80	3.2	4.6	6.85			
$\Delta B_\parallel^{expt}$(G)	1.5 ± 0.15	1.55 ± 0.15	1.95 ± 0.2	1.85 ± 0.15	3.25 ± 0.2	4.8 ± 0.3	6.85 ± 0.3			

TABLE IV. Experimental and calculated linewidths of the EPR spectra of Pb^{3+} in calcite at 285 GHz and their temperature dependences for samples I and II.

T (K)	50^I	50^{II}	85^{II}	110^I	135^{II}	150^{II}	180^{II}	230^I	295^I
δA(G)	4.7±0.25	4.7±0.25	4.7±0.25	4.8±0.25	5.2±0.25	5.7±0.25	6.5±0.25	8.1±0.25	9.0±0.5
ΔB_0^{Gc}(G)	−0.7±0.1	−0.7±0.1	−0.7±0.1	−0.8±0.15	0.85±0.2	0.9±0.2	1.0±0.2	−1.3±0.2	−2.0±0.3
ΔB_0^{GnI}(G)	0.5±0.1			0.5±0.1				0.5±0.1	0.5±0.1
ΔB_0^{GnII}(G)		1.0±0.2	1.0±0.2		1.0±0.2	1.0±0.2	1.0±0.2		
d_D^2(G)	200±50	200±50	300±50	400±50	470±50	520±50	700±75	1070±100	1350±100
ΔB_0^{calc}(G)	1.05	1.45	1.5	1.70	3.0	3.9	6.5	9.8	15.0
ΔB_0^{expt}(G)	1.1±0.1	1.55±0.15	1.70±0.2	1.9±0.2	3.2±0.2	4.2±0.25	6.6±0.25	9.8±0.3	14.8±1
ΔB_1^{calc}(G)	2.55	2.80	2.85	3.25	4.65	5.75	8.35	13.05	18.4
ΔB_1^{expt}(G)	2.6±0.2	2.80±0.2	3.1±0.25	3.3±0.25	4.95±0.3	5.6±0.3	8.7±0.35	13.15±0.4	18.6±1
ΔB_2^{calc}(G)	3.1	3.20	3.45	3.75	5.6	6.25	9.0	13.45	18.4
ΔB_2^{expt}(G)	3.1±0.2	3.0±0.2	3.35±0.2	3.75±0.2	5.4±0.3	6.5±0.25	8.9±0.35	13.75±0.4	17.5±1
$\Delta B_\parallel^{calc}$(G)	1.45	1.95	2.35	2.8	3.6	4.4			
$\Delta B_\parallel^{expt}$(G)	1.25±0.2	2.05±0.2	2.2±0.2	2.6±0.2	3.35±0.3	4.2±0.4			

Figures 3(a) and 3(b) illustrate the temperature dependence of the linewidth for the perpendicular detected transition B_1 measured at 190 and 285 GHz, respectively. At both frequencies Eq. (4.2) gives a satisfactory fit of the experimental data. Analogous results were obtained for the perpendicular detected transition B_2. The second term on the right-hand side of Eq. (4.2) shows a linear dependence on temperature and thus corresponds to a direct SLR process (see Tables II, III, and IV). It must be originated by MHF for two reasons: (i) ΔB_0 does not exhibit similar effects and (ii) it has approximately a linear dependence on ν^2. Figure 4 shows the frequency dependence of the relaxation by MHF at $T=100$ K. At this temperature, the Raman relaxation contribution by MHF is very small compared to the direct relaxation process by MHF. The observed frequency dependence can be explained by Eq. (3.22a). A direct relaxation mechanism by MHF is expected to be proportional to the phonon spectral density of the lattice $\rho(\nu)$. In the Debye approximation at low frequency $\rho(\nu)$ has a ν^2 dependence.[12,15] At 95 GHz, the observed linewidth is smaller than the calculated value (see Fig. 4). This fact shows that, as observed by infrared spectroscopy,[30] at relatively high frequency, $\rho(\nu)$ has not exactly a ν^2 dependence. The direct relaxation process by MHF dominates the SLR rates at $T<100$ K. At frequencies higher than 95 GHz, the direct SLR rate dominates over Raman relaxation process by MHF. At 95 GHz and high temperature, these two processes are instead of comparable size.

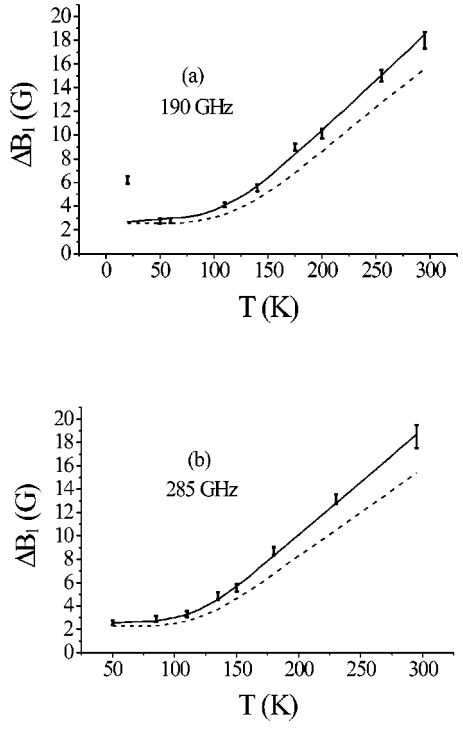

FIG. 3. Temperature dependence of ΔB_1 (a) at 190 GHz and (b) at 285 GHz. The solid lines are calculated with the present theory. The dashed lines are calculated without the contribution of the direct relaxation process by MHF. The experimental and calculated values do not include the magnetic field inhomogeneity.

At $T<50$ K, the perpendicular detected transitions B_1, and B_2 are, as the B_0 transition, strongly saturated [see Table III and Fig. 3(a)]. In this condition in fact for $^{207}Pb^{3+}$ ions the direct relaxation rate by MHF is much faster than the relaxation rate by MSO, i.e., $d^2 \gg k^2$, and from Eq. (3.26b),

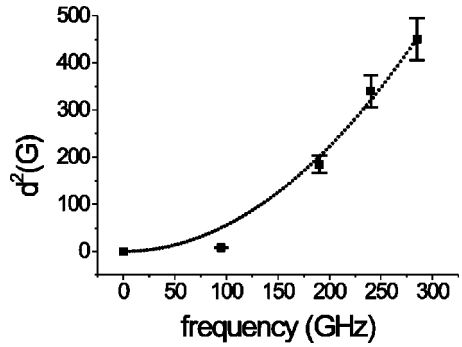

FIG. 4. Frequency dependence at 100 K of the direct relaxation rate by MHF.

$$^{sat}(T_1^{14,23})^{-1} \cong (T_1^0)^{-1} = k^2. \tag{4.3}$$

At high temperature, the Raman SLR process is important. The Lorentzian linewidths of the perpendicular detected transitions B_1 and B_2 are expected to be narrower than the values predicted by the Redfield theory. However, since $d_R^2 \ll d_d^2$ and at high magnetic fields $\gamma^2 \ll 1$, the contribution of the perturbation terms higher than the second order is negligible. Moreover, since the distance of the resonance fields of the two HF components B_1 and B_2 is about 1.4 T (38 GHz), $\gamma^2(B_2) < \gamma^2(B_1)$. Although $\gamma^2 \ll 1$, the contribution to the Lorentzian linewidth of the direct relaxation by MHF is important, as shown in Fig. 3, because d_d^2 is very large at 190 and 285 GHz. Consequently, from Eqs. (3.6a), (3.21), and (4.2), at all the frequencies $\Delta B_1^L > \Delta B_2^L$. The fact that, at 285 GHz, ΔB_2 is slightly larger than ΔB_1 (see Table IV) is due to a Gaussian contribution. The linewidths of the perpendicular detected transitions were satisfactorily fitted, allowing correlation among the δg and δA parameters in Eq. (3.3). The minus sign for δg compared to δA in Tables II, III, and IV means that δg and δA have opposite signs. This is the reason why at 285 GHz, being $\Delta B_2^{Gc} > \Delta B_1^{Gc}$, ΔB_2 is a little larger than ΔB_1. For the perpendicular detected transitions in Eq. (3.2), $(\Delta B_{1,2}^{Gc})^2 \gg (\Delta B_{1,2}^{Gn})^2$.

3. High-field multifrequency LWD analysis of the parallel detected transition for $^{207}Pb^{3+}$

Due to the experimental configuration and in particular the lack of a resonator in the high-frequency spectrometer, it was possible to observe the parallel-detected transition. As far as the contributions of the different SLR mechanisms are concerned, there are two important differences between the parallel- and perpendicular-detected transitions. The first one is related to the contributions of the different SLR processes to the Lorentzian components of the linewidth under nonsaturation conditions. The second difference concerns the saturation of these transitions.

In Fig. 5 is shown the temperature dependence of the linewidth of the parallel transition at 190 and 285 GHz. The solid line is calculated with Eq. (3.23d), while the dashed line is calculated not including the contribution of the direct SLR process d_D^2. As one can see in Figs. 3, and 5, and in Eqs. (3.23), (3.24), and (3.20), the contribution to the linewidth of d_D^2 is 2 times stronger for the parallel- than for the perpendicular-detected transitions. At high temperature, the contribution of the direct process to the linewidth is comparable to that of the Raman process. At $T < 77$ K, the contributions of the Raman SLR processes k_R^2 and d_R^2 to the linewidth are negligible. The direct process d_D^2 defined in Eq. (3.22a) instead contributes significantly to the linewidth of $B_\parallel$ even at lower temperatures. This is the reason why at 190 GHz, the $B_\parallel$ line becomes narrower by decreasing the temperature from 60 K to 20 K (see Table III and Fig. 5).

At low temperature the perpendicular-detected transitions are much more easily saturated than the parallel one. At $T < 50$ K, in fact, $d^2 \gg k^2$. Thus, from Eq. (3.26c), for the $B_\parallel$ transition,

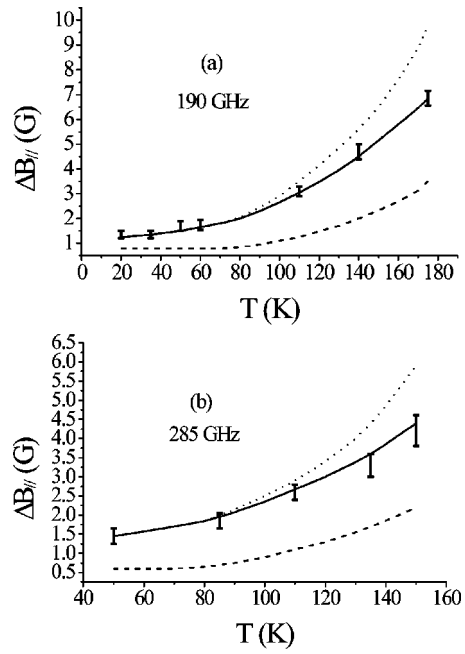

FIG. 5. Temperature dependence of $\Delta B_\parallel$ (a) at 190 GHz and (b) at 285 GHz. The solid lines are calculated with the present theory. The dashed lines are calculated without the contribution of the direct relaxation process by MHF. The dotted lines correspond to the Redfield theory. The experimental and calculated values do not include the magnetic field inhomogeneity.

$$^{sat}(T_1^{13})^{-1} \cong 2\alpha^2\gamma^2(\alpha^2-\gamma^2)^2 d^2. \tag{4.4}$$

The ratio between the saturation factors relative to the perpendicular- and parallel-detected transitions is

$$\frac{\langle p_{14}^2\rangle (T_2^{14})^{-1} T_1^{14}}{\langle p_{13}^2\rangle (T_2^{13})^{-1} T_1^{13}} \cong \frac{\alpha^2(\alpha^2-\gamma^2)^2 b_\perp^2 d^2}{2 b_{||}^2 k^2} \cong \frac{b_\perp^2 d^2}{2 b_{||}^2 k^2} \gg 1, \tag{4.5}$$

because at $\nu > 95$ GHz, $\alpha^2 \gg \gamma^2$, and in our experimental setup the perpendicular and parallel components of the magnetic amplitude of the oscillating field in the sample are comparable.

As a result, the LWD analysis and the saturation of the EPR transitions in our system confirm that the direct SLR process by MSO, k_D^2, is negligible in comparison with the direct SLR process by MHF, d_D^2. Similar results were observed for other Kramers ions.[31,32]

At high fields, the contributions of the perturbation terms higher than the second order to the Lorentzian linewidth of the perpendicular-detected transitions are negligible. On the contrary, for the parallel-detected transition this contribution is very important, as shown in Eq. (3.23d). Figure 5 shows that at 190 GHz and 285 GHz the Redfield theory, represented by the dotted line, predicts larger values of $\Delta B_\parallel$ than the measured ones, especially at high temperature.

Besides the Lorentzian contributions, Gaussian contributions have been considered. $\Delta B_{||}^{Gn}$ depends on the sample dimension, while $\Delta B_{||}^{Gc}$ is given by Eq. (3.3d). Since δg and δA are correlated and have opposite signs, at 285 GHz

$(\Delta B_{||}^{Gc})^2 \ll (\Delta B_{||}^{Gn})^2$. Therefore as far as the Gaussian component at 285 GHz is concerned $\Delta B_{||}^{G} \cong \Delta B_{||}^{Gn}$. $\Delta B_{||}^{GnII}$ is about 2 times larger than $\Delta B_{||}^{GnI}$, which explains the difference reported in Table IV between the linewidths observed at 285 GHz for the two samples at 50 K. At all the used frequencies and for all the transitions, $\Delta B_i^{Gn} \cong x_{I,II} \times B_i$. For the smaller crystal $x_I \cong 0.5 \times 10^{-5}$, while for the larger one $x_{II} \cong 10^{-5}$. As the larger crystal is a rhombohedron of about 1 cm, we obtained a value of the homogeneity x of the magnet of about 10 ppm in a 1-cm-diam spherical volume, which confirms the specification of the supplier (Oxford Instruments, U.K.).

δg and δA have temperature dependences analogous to that of the HF interaction,[13]

$$\delta A(T) = \delta A(0)\left(1 + \delta a \coth\frac{\hbar\omega^R}{2kT}\right), \tag{4.6}$$

and an analogous expression for δg, where ω^R is the frequency of the resonant mode associated with the lead impurity in calcite. In the above equations $\hbar\omega^R \cong \theta k$, where θ can be found from the temperature dependences of the Raman SLR processes given by Eq. (3.18). While A decreases if the temperature increases, δg and δA both increase with the temperature. The vibration mode mixes excited states into the ground s orbital of the Pb^{3+}. Consequently, the s character decreases, and the Fermi contact HF interaction A decreases too. The lower-symmetry positions due to the local defects generate a similar effect. Thus, $\delta A(0)$ corresponding to the static local defects and δa corresponding to the changes in the vibration properties due to the local defects have the same signs. For Pb^{3+} in calcite, $g_{||}$ and $g_{\perp}$ are both larger than the free-electron g value 2.0023. An increasing of g corresponds to a decreasing of the s character of the Pb^{3+} orbital and to a decreasing of A. That is why δg and δA have opposite signs in Eqs. (3.3). The fact that δg and δA are correlated in Eqs. (3.3) proves that they have the same physical origin. Therefore it is expected that δg and δA strains are mainly due to a large resonant mode of frequency ω^R. This normal mode dominates the vibration properties of the Pb^{3+} impurity in calcite. Consequently, all three dynamic effects in the EPR spectra of Pb^{3+} in calcite—the temperature dependence of the HF interaction, of the Lorentzian, and of the Gaussian linewidth—are correlated with the presence of this resonant mode.

V. CONCLUSIONS

EPR studies in a wide temperature and frequency range allowed a detailed investigation of the relaxation process in a multilevel spin system. The different mechanisms operative in the SLR phenomena could be disentangled by this multifrequency study and the related theory[25] successfully tested. From the LWD analysis of the HF[2]EPR spectra of Pb^{3+} in calcite we can draw the following conclusions: (i) The high-frequency Lorentzian component of the linewidth corresponding to the Pb^{3+} with zero nuclear spins is the same as that measured at low frequencies. However, unlike the low-field case, at high fields there is a Gaussian component due to the strain of the Zeeman interaction and the inhomogeneity of the magnetic field. (ii) For $^{207}Pb^{3+}$, which is a multilevel spin system, there are two relevant new features: (a) the direct relaxation mechanism by MHF significantly contributes to the linewidths even at room temperature and (b) the SLR time of a simple transition measured from the linewidth under conditions of negligible saturation could be very different from that measured by the continuous saturation method. (iii) Since the frequency of the oscillating field is higher than the zero-field splitting, it becomes possible to observe and analyze the parallel-detected transition. This analysis makes a clear distinction between the contribution of the SLR mechanism originated by the modulation of the HF interaction and of the spin-orbit interaction to the linewidth of the parallel- and perpendicular-detected transitions. Concerning this distinction we emphasize the following: (a) the contribution of the Raman relaxation mechanisms by MSO to the linewidth of the parallel-detected transition is 2 times weaker than the contribution to the linewidth of the perpendicular-detected transitions. This is in agreement with a recent theory of relaxation.[25] (b) The contribution of the direct relaxation rate by MHF is 2 times larger for the parallel-detected transition than for the perpendicular-detected transitions. (c) A much more important difference was observed for the SLR times that characterize the saturation of these transitions at low temperatures. Thus, the perpendicular-detected transitions are much more easily saturated than the parallel-detected transition. This proves that although the SLR times obtained by different methods depend only on the SLR rates w_{ij}, their measured values could be very different.

ACKNOWLEDGMENTS

We thank M. Dragusin for the γ-ray irradiation. This work was supported by NATO Collaborative linkage Grant No. PST.CGL.976969. We gratefully acknowledge also financial support by the Consiglio Nazionale delle Ricerche (C.N.R.) Italy and the National Council for University Research (C.N.C.S.I.S.) Romania. The Access to research Infrastructure action of the Improving Human Potential Program of the European Community is gratefully acknowledged for the Contract No. HPRI-CT-2000-40022 (SENTINEL).

[1] G.R. Eaton and S.S. Eaton, Appl. Magn. Reson. **16**, 161 (1999).
[2] G. R. Eaton, S. S. Eaton, and K. M. Salikhov, *Foundations of Modern EPR* (World Scientific, Singapore, 1998).
[3] Ya.S. Lebedev, Appl. Magn. Reson. **7**, 339 (1995).
[4] A.L. Barra, L.C. Brunel, D. Gatteschi, L. Pardi, and R. Sessoli, Acc. Chem. Res. **31**, 460 (1998).
[5] J.H. Freed, Annu. Rev. Phys. Chem. **51**, 655 (2000).
[6] T.F. Prisner, Adv. Magn. Opt. Reson. **20**, 245 (1997).

[7] K. Möbius, Chem. Soc. Rev. **29**, 129 (2000).
[8] E.J. Reijerse, P.J. van Dam, A.A.K. Klaassen, W.R. Hagen, P.J.M. van Bentum, and G.M. Smith, Appl. Magn. Reson. **14**, 153 (1998)).
[9] G. M. Smith and P. C. Riedi, *Electron Paramagnetic Resonance*, *Progress in High Field EPR*, Vol. 17 (The Royal Society of Chemistry, London, 2000), pp. 164–204.
[10] A. Bencini and D. Gatteschi, Trans. Met. Chem. **8**, 1 (1982).
[11] B.R. McGarvey, Trans. Met. Chem. **3**, 89 (1966).
[12] A. Abragam and B. Bleany, *Electron Paramagnetic Resonance of Transition Ions* (Clarendon Press, New York, 1970).
[13] F.F. Popescu and V.V. Grecu, Phys. Status Solidi B **68**, 595 (1975).
[14] L. Banci, I. Bertini, and C. Luchinat, Magn. Reson. Rev. **11**, 1 (1986).
[15] K. J. Standley and R. A. Vaughan, *Electron Spin Relaxation Phenomena in Solids* (Hilger, London, 1969).
[16] F.F. Popescu and V.V. Grecu, J. Phys. C **15**, 1547 (1982).
[17] S.V. Nistor, D. Schoemaker, and I. Ursu, Phys. Status Solidi B **185**, 9 (1994), and references therein.
[18] J. Huang, N.D. Chasteer, and J.J. Fitzgerald, Chem. Mater. **10**, 3848 (1998).
[19] B. Andlauer, I. Schneider, and W. Tolksdorf, Phys. Rev. B **8**, 1 (1973).
[20] G. Annino, M. Cassettari, M. Fittipaldi, L. Lenci, I. Longo, M. Martinelli, C.A. Massa, and L.A. Pardi, Appl. Magn. Reson. **19**, 495 (2000).
[21] A.M. Stoneham, J. Phys. D **5**, 670 (1972).
[22] F. Bloch, Phys. Rev. **102**, 104 (1956); **105**, 206 (1957).
[23] A.G. Redfield, IBM J. Res. Dev. **1**, 19 (1957); in *Advance in Magnetic Resonance*, edited by J. S. Waugh (Academic Press, New York, 1965), Vol. 1.
[24] A. Abragam, *The Principles of Nuclear Magnetism* (Oxford University Press, New York, 1961).
[25] F.F. Popescu, Phys. Status Solidi B **214**, 113 (1999).
[26] F.F. Popescu and V.V. Grecu, J. Phys. C **15**, 1531 (1982).
[27] J. Murphy, Phys. Rev. **145**, 241 (1966).
[28] D.W. Feldman, J.G. Castle, and G.R. Wagner, Phys. Rev. **145**, 237 (1966).
[29] F.F. Popescu, Phys. Rev. B **48**, 13 569 (1993).
[30] A.S. Barker and A.J. Sievers, Rev. Mod. Phys. **47**, Suppl. 2, 1 (1975).
[31] G.H. Larson and C.D. Jeffries, Phys. Rev. **145**, 311 (1966).
[32] H. Panepucci and L.F. Mollenauer, Phys. Rev. **178**, 589 (1969).